X-ray emission from star-forming galaxies - III. Calibration of the $L_X - $ SFR relation up to redshift $z \approx 1.3$

S. Mineo[1,2]⋆, M. Gilfanov [2,3] and R. Sunyaev [2,3]

[1] *Harvard-Smithsonian Center for Astrophysics, 60 Garden Street Cambridge, MA 02138, USA*
[2] *Max Planck Institut für Astrophysik, Karl-Schwarzschild-Str. 1 85741 Garching, Germany*
[3] *Space Research Institute of Russian Academy of Sciences, Profsoyuznaya 84/32, 117997 Moscow, Russia*

ABSTRACT

We investigate the relation between total X-ray emission from star-forming galaxies and their star formation activity. Using nearby late-type galaxies and ULIRGs from Paper I and star-forming galaxies from *Chandra* Deep Fields, we construct a sample of 54 galaxies spanning the redshift range $z \approx 0 - 1.3$ and the SFR range $\sim 0.1 - 10^3 \, M_\odot \, \mathrm{yr}^{-1}$. In agreement with previous results, we find that the $L_X - $ SFR relation is consistent with a linear law both at $z = 0$ and for the $z = 0.1 - 1.3$ CDF galaxies, within the statistical accuracy of ~ 0.1 in the slope of the $L_X - $ SFR relation. For the total sample, we find a linear scaling relation $L_X / \mathrm{SFR} \approx (3.5 \pm 0.4) \times 10^{39} (\mathrm{erg \, s}^{-1}) / (M_\odot \, \mathrm{yr}^{-1})$, with a scatter of ≈ 0.4 dex. About $\sim 3/4$ of the 0.5–8 keV luminosity generated per unit SFR is provided by HMXBs. We find no statistically significant trends in the L_X / SFR ratio with the redshift or star formation rate and constrain the amplitude of its variations by $\lesssim 0.1 - 0.2$ dex. These properties make X-ray observations a powerful tool to measure the star formation rate in normal star-forming galaxies that dominate the source counts at faint fluxes.

Key words: X-rays: galaxies – galaxies: star formation – galaxies: starburst – X-rays: ISM – X-rays: binaries.

1 INTRODUCTION

High-mass X-ray binaries (HMXBs) and the hot ionized inter-stellar medium (ISM) are the main contributors to the total X-ray output of normal (i.e. not containing a luminous active galactic nucleus (AGN)) star-forming galaxies. It is well established that the collective X-ray luminosity of HMXBs well correlates with the star formation activity of the host galaxy (Grimm, Gilfanov, & Sunyaev 2003; Ranalli, Comastri, & Setti 2003; Lehmer et al. 2010; Mineo, Gilfanov, & Sunyaev 2011, 2012, hereafter Paper I). The hot ionized ISM contributes about $\sim 1/4$ to the observed X-ray emission from late-type galaxies in the standard X-ray band, its luminosity has been also shown to scale linearly with star formation rate (SFR) (Grimes et al. 2005; Li & Wang 2012; Mineo, Gilfanov, & Sunyaev 2012, hereafter Paper II). Thus, it has been proposed that the total, integrated X-ray luminosity from star-forming galaxies can be used as a proxy of the SFR (Grimm, Gilfanov, & Sunyaev 2003; Ranalli, Comastri, & Setti 2003). Although not entirely free from its own systematic uncertainties and contaminations, the X-ray based SFR proxy is less affected

by the interstellar extinction and cosmological passband redshift, than conventional SFR indicators. Furthermore, the $L_X - $ SFR scaling relation does not experience significant cosmological evolution up to redshifts of $z \sim 1 - 2$. This has been initially suggested based on direct measurements of the L_X / SFR ratios for several galaxies in Chandra deep fields (Grimm, Gilfanov, & Sunyaev 2003; Lehmer et al. 2010; Mineo, Gilfanov, & Sunyaev 2012) and was further supported by calculations of the maximal contribution of X-ray faint star-forming galaxies to the unresolved part of the Cosmic X-ray background (Dijkstra et al. 2012) and stacking analysis results (Cowie, Barger, & Hasinger 2012). These properties make the X-ray based SFR proxy a powerful tool to measure the star formation rate in distant galaxies.

The most significant systematic effect which can compromise the X-ray-based SFR measurements is the contamination by the emission of the central supermassive black hole, the AGN. Indeed, even low luminosity AGN, with $\log(L_X) \sim 42$ can outshine a $\sim 100 M_\odot / \mathrm{yr}$ starburst. As populations of bright galaxies are mainly composed of AGN (for recent results, see e.g. Xue et al. 2011; Lehmer et al. 2012), SFR measurements using X-ray luminosity can be applied only to a relatively small fraction of bright galaxies. In this

case, a careful investigation of the nature of each galaxy is required in order to separate late-type from early-type galaxy populations. On the contrary, among faint sources, $F_X \lesssim 10^{-17}$ erg/s/cm^2, the majority are star-forming galaxies located at moderate and large redshifts, $z \sim 0.5 - 3$ (Cowie, Barger, & Hasinger 2012; Lehmer et al. 2012). This makes the X-ray based SFR proxy a powerful tool to measure the star formation rate in faint galaxies, where it can be used *en masse*, to infer the cosmic star formation history (e.g. Cowie, Barger, & Hasinger 2012).

The aim of this paper is to obtain the $L_X - $ SFR scaling relation for the *total* X-ray luminosity and to investigate its behavior in a broad range of redshifts. For the redshift $z = 0$, we use the sample of star-forming galaxies and ULIRGs (ultra-luminous infrared galaxies) from Papers I and II. We then select normal star-forming galaxies from the *Chandra* Deep Fields (CDF) expanding the local sample towards cosmologically interesting redshifts and high star formation rates. We combine these data in order to calibrate the $L_X - $ SFR scaling relation in a broad range of redshifts and star formation rates.

The structure of the paper is as follows. In Section 2 we briefly summarize the selection criteria and properties of the local sample. In Section 3 we describe selection of late-type galaxies from the *Chandra* Deep Fields data and the procedures used to calculate their X-ray luminosities and star formation rates. The $L_X - $ SFR relation is derived in the Section 4 and its redshift dependence is investigated in the Section 5. In the Section 6 we summarize our findings.

Throughout this paper we assume flat ΛCDM cosmology with $H_0 = 70$ km/s/Mpc, $\Omega_M = 0.3$ and $\Omega_\Lambda = 0.7$.

2   LOCAL GALAXIES

2.1   The sample

We constructed the local sample of star-forming galaxies by merging the sample of nearby galaxies resolved by *Chandra* from Paper II (Sect. 2, Table 1), and the sample of unresolved LIRGs (luminous infrared galaxies) and ULIRGs defined in Paper I (Sect. 2.2, Table 2). The local sample contains 29 star-forming galaxies, their parameters are summarized in Table 1.

The star formation rates and stellar masses ($M_\star$) were determined in the Paper I, based on far-infrared, UV and K-band luminosities. These quantities were measured for the same spatial regions as used for computing the X-ray luminosity, defined in the Sect. 5 of Paper I. The star formation rates and stellar masses of the local sample span broad ranges, from $\sim 0.1 - 290\ M_\odot$ yr^{-1} and $\sim 3 \times 10^8 - 2 \times 10^{11}\ M_\odot$ respectively.

2.2   Total X-ray luminosity

The data preparation was done following the standard CIAO[1] threads (CIAO version 3.4; CALDB version 3.4.1), exactly in the same way as described in Sect. 3 of Paper I.

For resolved galaxies, listed in the first part of the Table 1, the source spectra were extracted in the 0.5–8 keV energy
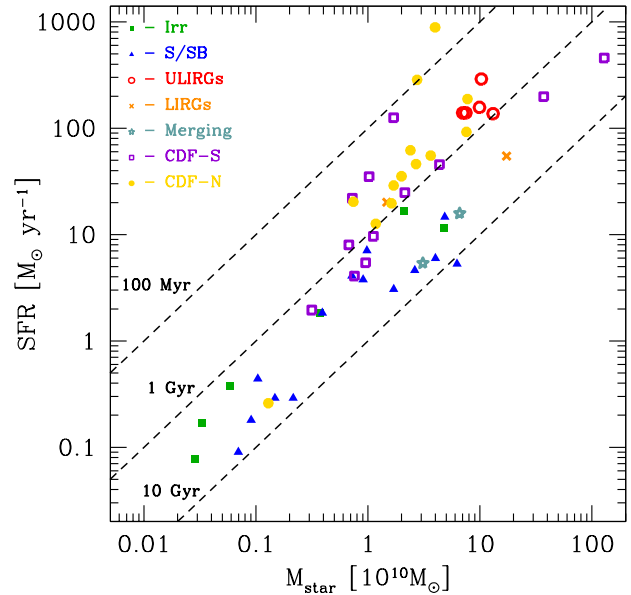
[1] http://cxc.harvard.edu/ciao3.4/index.html

Figure 1. The SFR $- M_\star$ plane. Different types of galaxies are plotted with different symbols: Irregulars in (green) filled squares, spirals in (blue) filled triangles, ULIRGs in (red) empty circles, LIRGs in (orange) crosses, interacting systems in (grey) empty stars. Star-forming galaxies from *Chandra* Deep Fields -South and -North are plotted as empty squares (purple) and filled circles (gold) respectively. The dashed lines correspond to constant stellar-mass-to-SFR ratio.

band and the background spectra were created as described in Sect. 3.3 of Paper II. Spatial regions for extracting source spectra are defined in the Paper I. Both source and background spectra and the associated ARF and RMF files were produced by using `specextract` script and modeled using XSPEC v. 12.3.1x. The spectra were grouped in order to have minimum 15 counts per channel to apply the χ^2 fitting. For most of the spectra a good fit was obtained with a two component model: a thermal plasma (`mekal`) plus a power-law, corrected for the Galactic absorption. A second photoelectric absorption, accounting for the intrinsic absorption and/or a second thermal component was required for some of the galaxies. It was decided based on the result of the F-test, using the probability of 10^{-3} as the threshold (see Paper II for details). For each galaxy, we used the best fit model to calculate the count-to-erg conversion coefficient. Using this coefficient, the energy flux was computed form the background subtracted source count rate.

For the sample of unresolved starburst galaxies presented in the second part of Table 1, we adopted 0.5–8 keV luminosities from the Paper I.

3   STAR-FORMING GALAXIES FROM CHANDRA DEEP FIELDS

In order to extend the $L_X - $ SFR relation towards higher redshifts and star formation rates, we selected a sample of late-type galaxies in the Chandra Deep Fields. We started from the samples studied by Lehmer et al. (2008), who se-

Table 1. The local ($z = 0$) sample of star-forming galaxies.

Galaxy	D (Mpc)	Ref.[a]	Hubble type	SFR[b] ($M_\odot$ yr^{-1})	$M_\star$[c] ($10^{10}\,M_\odot$)	$\log L_{\rm X}^{\rm tot}$[d] (erg s^{-1})
			RESOLVED GALAXIES			
NGC 0278	$11.8^{+2.4}_{-2.0}$	(2)	SAB(rs)b	4.1	0.7	39.52
NGC 0520	$27.8^{+5.6}_{-4.7}$	(2)	Pec	11.6	4.7	40.53
NGC 1313	4.1 ± 0.2	(3)	SB(s)d	0.44	0.1	39.75
NGC 1569	1.9 ± 0.2	(4)	IB	7.8×10^{-2}	2.8×10^{-2}	38.17
NGC 2139	$26.7^{+5.8}_{-4.8}$	(5)	SAB(rs)cd	3.8	0.91	40.48
NGC 3079	18.2	(1)	SB(s)c	6.0	4.0	40.30
NGC 3310	19.8	(1)	SAB(r)bc pec	7.1	0.98	41.02
NGC 3556	$10.7^{+1.9}_{-1.6}$	(11)	SB(s)cd	3.1	1.7	39.87
NGC 3631	24.3 ± 1.6	(7)	SA(s)c	4.6	2.6	40.79
NGC 4038/39	13.8 ± 1.7	(8)	-	5.4	3.1	40.57
NGC 4194	$39.1^{+7.9}_{-6.6}$	(2)	IBm pec	16.8	2.1	40.92
NGC 4214	2.5 ± 0.3	(9)	IAB(s)m	0.17	3.3×10^{-2}	38.53
NGC 4490	$7.8^{+1.6}_{-1.3}$	(2)	SB(s)d pec	1.8	0.39	40.32
NGC 4625	$8.2^{+1.7}_{-1.4}$	(2)	SAB(rs)m pec	0.09	7.0×10^{-2}	37.92
NGC 5253	4.1 ± 0.5	(6)	Im pec	0.38	5.9×10^{-2}	38.31
NGC 5474	6.8	(10)	SA(s)cd pec	0.18	9.1×10^{-2}	39.05
NGC 5775	$26.7^{+11.9}_{-8.2}$	(2)	Sb(f)	5.3	6.3	40.88
NGC 7090	7.6	(1)	SBc	0.29	0.22	39.08
NGC 7541	$34.9^{+6.6}_{-5.7}$	(5)	SB(rs)bc pec	14.7	4.9	40.39
NGC 7793	$4.0^{+0.7}_{-0.6}$	(11)	SA(s)d	0.29	0.15	38.53
UGC 05720	$24.9^{+11.1}_{-7.7}$	(2)	Im pec	1.8	0.37	39.77
			UNRESOLVED GALAXIES			
IRAS 17208-0014	183.0	(1)	ULIRG	289.9	10.3	41.40
IRAS 20551-4250	179.1	(1)	ULIRG	139.4	7.5	41.63
IRAS 23128-5919	184.2	(1)	ULIRG	139.6	7.0	41.88
IRAS 10565+2448	182.6	(1)	ULIRG	156.8	9.9	41.42
IRAS 13362+4831	120.9	(1)	LIRG	54.8	17.3	41.81
IRAS 09320+6134	164.3	(1)	ULIRG	137.1	13.1	41.39
IRAS 00344-3349	84.0	(1)	LIRG	20.1	1.5	41.23
NGC 4676	98.2	(1)	-	15.8	6.6	40.92

[a] References for distances: (1) Sanders et al. (2003), (2) Tully (1988), (3) Grisé et al. (2008), (4) Makarova & Karachentsev (2003), (5) Willick et al. (1997), (6) Saha et al. (2006), (7) Ismail et al. (2005), (8) Saviane, Hibbard, & Rich (2004), (9) Drozdovsky et al. (2002), (10) Drozdovsky & Karachentsev (2000), (11) Tully et al. (2009).
[b] Star formation rate from Spitzer and GALEX data (see Sect. 6 Paper I).
[c] Stellar mass from 2MASS data (see Sect. 5 Paper I).
[d] Total X-ray luminosity of galaxies, i.e. gas and X-ray binary contribution, in 0.5–8 keV band, measured as described in Sect. 2.2.

lected late-type galaxies in the Chandra Deep Field-North (CDF-N) and Extended Chandra Deep Field-South (E-CDF-S), and by Xue et al. (2011), the 4 Ms Chandra Deep Field-South (4Ms CDF-S) survey. For the South field, the Lehmer et al. (2008) sample was based on 1 Msec centered on the Chandra Deep Field-South and four flanking fields 250 ksec each, while Xue et al. (2011) covered only the Chandra Deep Field-South but to 4 times larger depth.

These two samples were filtered according to the following criteria: (i) rigorous determination of the morphological type appropriate for a star-forming galaxy; (ii) availability of 0.5–8 keV X-ray flux measurement; (iii) availability of 1.4 GHz radio flux measurement for the SFR calculation or SFR determinations by Lehmer et al. (2008); (iv) the value of specific SFR (SFR/$M_\star$) larger than 10^{-10} yr^{-1}.

3.1 Selection by the morphological type

The sample from Lehmer et al. (2008) includes 225 X-ray sources. Among them, 121 are classified as AGN candidates, while the remaining 104 sources are classified as normal late-type galaxies based on their rest-frame optical colors. For the aims of our analysis, we applied two main selection criteria to the Lehmer et al. (2008) sample: we excluded *i*) all the AGN candidates and *ii*) objects detected only in one of the sub-bands, for which full band luminosity was not available. After this selection, 52 objects were left, 37 from the CDF-N and 15 from the E-CDF-S. As it was pointed out by Lehmer et al. (2012), a single color division does not perfectly disentangle the early-type and late-type galaxy populations. In order to exclude a possible early-type galaxy

Table 2. Late-type galaxies from the *Chandra* Deep Fields.

CXO	Redshift	Field[a]	Morph.[b] Type	$\log M_\star$ $(M_\odot)$	$\log L_{0.5-8\mathrm{keV}}$ (erg s^{-1})	$S_{1.4\mathrm{GHz}}$ (μJy)	$\log L_{1.4\mathrm{GHz}}$ (erg s^{-1})	SFR $(M_\odot \ \mathrm{yr}^{-1})$
J033206.42-274728.7	1.02	4Ms CDF-S	3	11.57	41.80	80.0	30.55	197.91
J033211.54-274713.3	0.58	4Ms CDF-S	6	10.23	41.08	201.0	30.35	125.73
J033217.90-275100.1	0.12	4Ms CDF-S	4	9.50	39.52	100.0	28.55	1.95
J033218.04-274718.8	0.73	4Ms CDF-S	8	12.11	41.59	524.0	30.92	457.02
J033220.28-275222.3	0.34	4Ms CDF-S	6	9.86	40.69	106.0	29.60	21.99
J033228.00-274639.7	0.25	4Ms CDF-S	6	9.83	40.01	86.0	29.16	7.98
J033229.88-274424.5	0.08	E-CDF-S	4	10.05	40.18	1130.0	29.24	9.61
J033229.99-274404.8	0.08	E-CDF-S	3	9.88	40.24	482.0	28.86	4.07
J033233.00-275030.2	0.67	E-CDF-S	4	10.64	41.42	42.0	29.91	45.52
J033236.18-274931.8	0.55	E-CDF-S	8	10.33	41.53	48.0	29.65	24.76
J033237.27-275127.5	0.69	4Ms CDF-S	6	10.01	41.23	41.0	29.80	34.96
J033238.82-274956.3	0.24	E-CDF-S	3	9.98	40.48	63.0	28.99	5.44
J123559.74+621550.3	0.38	CDF-N	4	10.56	41.28	212.0	30.00	55.25
J123619.47+621252.9	0.47	CDF-N	3	10.43	41.31	108.0	29.92	46.0
J123634.47+621213.4	0.46	CDF-N	8	10.88	41.53	233.0	30.22	92.28
J123632.45+621037.7	0.14	CDF-N	6	9.11	39.08	-	-	0.26[c]
J123634.53+621241.3	1.22	CDF-N	6	10.60	42.39	230.0	31.20	887.34
J123646.67+620833.6	0.97	CDF-N	3	10.89	41.93	80.1	30.53	188.27
J123649.72+621313.4	0.47	CDF-N	6	9.87	41.14	49.2	29.56	20.32
J123651.12+621031.2	0.41	CDF-N	4	10.23	41.10	95.0	29.72	28.89
J123652.83+621808.1	0.25	CDF-N	3	10.30	40.53	350.0	29.80	35.33
J123653.37+621140.0	1.27	CDF-N	8	10.44	42.30	65.7	30.71	285.27
J123659.92+621450.3	0.76	CDF-N	8	10.38	41.45	47.0	30.05	61.93
J123708.32+621056.4	0.42	CDF-N	6	10.07	41.26	45.1	29.36	12.64
J123716.82+621007.8	0.41	CDF-N	3	10.21	40.89	63.3	29.55	19.65

[a] References for redshift and fields: E-CDF-S and CDF-N galaxies are from Lehmer et al. (2008), 4Ms CDF-S galaxies are from Xue et al. (2011).
[b] Morphological Type from Bundy, Ellis, & Conselice (2005), according to the following classification: 3=Sab, 4=S, 6=Irr, 8=Merger.
[c] Determination from Lehmer et al. (2008) rescaled to Salpeter IMF for $0.1 - 100 \, M_\odot$ mass range.

contamination of the Lehmer et al. (2008) sample, we cross-matched the selected 52 sources with the morphological catalogs of galaxies in the GOODS North and South fields (Bundy, Ellis, & Conselice 2005). Using a match radius of 1.5″ we found a total of 44 pairs, 11 for the E-CDF-S and 33 for the CDF-N sample. Two galaxies of the latter sample (J123603.26+621111.3 and J123627.32+621258.1) are classified as early-type and were excluded. We also excluded eight galaxies without match in the GOODS catalogs, obtaining a final sample of 42 galaxies.

As a check, we cross-correlated the obtained sample of CDF-N sources with the "High-SFR sample" in Paper I (Table 3), which includes seven galaxies from the *Hubble Deep Field North* (HDF-N). For seven HDF-N sources, we found six counterparts. The remaining galaxy, 123716.3+621512, was not present in the GOODS catalog. Correspondingly, we did not include it in our analysis.

The 4 Ms Chandra Deep Field-South (CDF-S) survey (Xue et al. 2011) includes 740 X-ray sources, of which 578 are classified as AGN and 162 as normal galaxies. Following same strategy as above, we excluded all AGN candidates as well as sources for which broad band X-ray luminosity was not available. Late-type galaxies from the E-CDF-S, already included in the Lehmer et al. (2008) sample, were not considered further. This shrank the sample to 94 galaxies. We cross-correlated these sources with the

morphological catalog of galaxies in the GOODS South field (Bundy, Ellis, & Conselice 2005). Using a match radius of 1.5″ we found 75 matches. Among them we selected only sources classified as late-type or merging galaxies. Sources with no match were excluded. The obtained sample from the 4 Ms Chandra Deep Field-South includes 48 star-forming galaxies.

After this selection we were left with a sample of 90 reliably identified star-forming galaxies from both Chandra Deep Fields. The sample will be reduced further after the cross-correlation with radio catalogs (see Sect. 3.3).

3.2   X-ray luminosity

Both Lehmer et al. (2008) and Xue et al. (2011) provide rest-frame X-ray luminosities in the 0.5–8 keV band. In both cases the K-correction was performed assuming a power spectrum. Lehmer et al. (2008) used a photon index $\Gamma = 2$, appropriate for star-forming galaxies, whereas Xue et al. (2011) used a photon index of $\Gamma = 1.8$, more appropriate for AGNs. For sources from the Lehmer et al. (2008) sample we used their original luminosity values. We recomputed luminosities for galaxies from Xue et al. (2011), using their fluxes and spectroscopic redshifts and adopting a photon index $\Gamma = 2$.

3.3 Star formation rate

The infrared (IR) and ultraviolet (UV) luminosities are good proxies of the star formation activity in late-type galaxies. However, the use of these two estimators for CDF galaxies is limited by both the lack of rest-frame UV spectroscopic data and the sensitivity limit of the available IR observations. For these reasons, Lehmer et al. (2008) were able only to compute upper limits on SFR for most of the sources in their galaxy sample. To measure star formation rates in the CDF galaxies, we used 1.4 GHz radio emission. It has been shown (e.g. Bell 2003; Schmitt et al. 2006) that this estimator is compatible with both IR- and UV-based estimators used for the local resolved galaxy sample (Sect. 2). We cross-correlated the X-ray sample of star-forming galaxies produced in the section 3.1 with catalogs of radio sources based on VLA observations of CDFs. For the CDF-N we used the Richards (2000) catalog, and Kellermann et al. (2008) catalog for the CDF-S. Using a match radius of $1.5''$ we found a total of 24 matches with VLA sources: 12 from CDF-N and 5 from E-CDF-S samples of Lehmer et al. (2008), 7 from the 4 Ms CDF-S sample of Xue et al. (2011). The radio flux densities $S_{1.4\,\mathrm{GHz}}$ were converted to luminosities using the standard procedure with K-correction. For the latter, we used radio spectral indices α as provided by VLA catalogues, except for 4 galaxies in CDF-N. For these sources we assumed a spectral index of $\alpha = 0.8$, according to Condon (1992). The radio-based SFRs were estimated using the calibration of Bell (2003):

$$\mathrm{SFR}\,(M_\odot\,\mathrm{yr}^{-1}) = 5.55 \times 10^{-29} L_{1.4\,\mathrm{GHz}}(\mathrm{erg\,s}^{-1}) \quad (1)$$

Among late-type galaxies without a radio counterpart in VLA catalogs, only one (J123632.45+621037.7) has an SFR determination in the catalog of Lehmer et al. (2008). For the rest of sources only upper limits on SFR were provided. For the galaxy mentioned above we used the SFR estimate by Lehmer et al. (2008), which is based on both IR and UV luminosities assuming a Kroupa (2001) IMF. We rescaled the SFR to the Salpeter IMF (a factor of ~ 2.1) for $0.1 - 100\,M_\odot$ mass range.

3.4 Stellar mass and specific star formation rate

As a final check, we verified that selected CDF galaxies satisfy the selection criterion applied for the sample of resolved galaxies in Paper I – that their specific SFR exceeds $\mathrm{SFR}/M_\star > 10^{-10}\,\mathrm{yr}^{-1}$.

This was rather straightforward for late-type galaxies selected from Lehmer et al. (2008), for which stellar mass measurements were available. For CDF-S galaxies from Xue et al. (2011), we used the multi-wavelength optical data provided in the same catalog. We calculated the stellar masses from the K-band luminosity and $(r-z)$ color calibration of the mass-to-light ratio from Zibetti, Charlot, & Rix (2009):

$$\log\left(\frac{M_\star}{M_\odot}\right) = \log\left(\frac{L_\mathrm{K}}{L_{\mathrm{K},\odot}}\right) - 1.405 + 1.157\,(r-z) \quad (2)$$

In particular, we derived $L_\mathrm{K}/L_{\mathrm{K},\odot}$ based on K-band AB magnitudes from the MUSYC catalog (Taylor et al. 2009), and computed $(r-z)$ colors based on AB magnitudes in R-band from the ESO 2.2 m WFI R-band
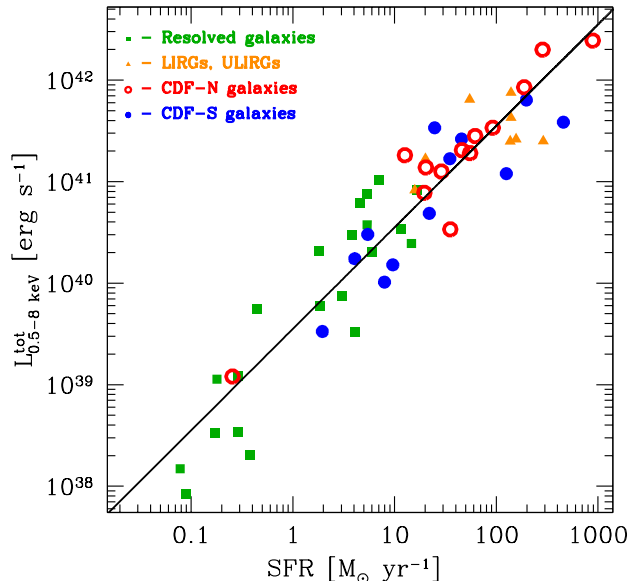

Figure 2. The $L_\mathrm{X}^\mathrm{tot} - \mathrm{SFR}$ relation. The (green) squares indicate galaxies from the local ($z = 0$) resolved sample, the (orange) triangles are LIRGs and ULIRGs from the unresolved sample, described in Sect. 2 and presented in Table 1. The filled (blue) circles are late-type galaxies from the Chandra Deep Field South and the and empty (red) circles are late-type galaxies from the Chandra Deep Field North, selected as described in Sect. 3 and presented in Table 2. The solid line shows the linear scaling relation, obtained using the whole sample of 54 galaxies and given by eq. (3).

catalog (Giavalisco et al. 2004), and z-band magnitudes from the GOODS-S Hubble Space Telescope (HST) catalog (Giavalisco et al. 2004).

All the sources which reached this step satisfied to the $\mathrm{SFR}/M_\star > 1 \times 10^{-10}\,\mathrm{yr}^{-1}$ criterion.

3.5 The final CDF sample

The final CDF sample consists of 25 galaxies from the *Chandra* Deep Fields, 13 objects from CDF-North and 12 from CDF-South. They are listed in Table 2, along with their parameters.

The entire sample, including 21 local (resolved) galaxies, 8 LIRGs and ULIRGs and 25 CDF galaxies (54 galaxies in total) is shown in the SFR–M_* plane in the Fig.1.

4 L_X − SFR RELATION FOR TOTAL LUMINOSITY

We approximate the $L_\mathrm{X}^\mathrm{tot} - \mathrm{SFR}$ data (in Fig.2) with the log-linear model $\log L_\mathrm{X}^\mathrm{tot} = \log K + \beta \log \mathrm{SFR}$. This model was applied to local sample and CDF sample separately. Both slope β and normalization K were set as free parameters of the fit. To fit the data we used least square minimization. The results are given in Table 3, which demonstrates that the best fit parameters for the local and CDF samples are compatible. We therefore performed the joint fit to the whole

Table 3. Summary of the parameters for $L_X - $ SFR relations obtained from least-squares fit.

Sample	FREE SLOPE			LINEAR FIT	
	$\log K$	β	σ (dex)	$\log K$	σ (dex)
$z = 0$ galaxies	39.53 ± 0.09	1.04 ± 0.08	0.42	39.56 ± 0.08	0.42
CDF galaxies	39.62 ± 0.15	0.95 ± 0.09	0.33	39.54 ± 0.07	0.33
all	39.55 ± 0.08	1.00 ± 0.05	0.38	39.55 ± 0.05	0.38

Note. The parameters are relative to the least-squares fit to the data with the relation $\log L_X = \log K + \beta \log$ SFR, respectively setting the slope β free and fixing it to unity. σ is the dispersion around the best-fitting relation. See Sect. 2.2 and 3.2 for the definition of the X-ray luminosities, Sect. 6 of Paper I and 3.3 of present work for the definition of SFR for $z = 0$ sample and CDF galaxies respectively.

sample of star-forming galaxies that includes both local and CDF sources, using same model. We obtained a slope $\beta = 1.00 \pm 0.05$, suggesting a linear relation. The linear scaling relation obtained by fixing the slope to unity is shown in Fig. 2 and it is given by the following equation:

$$L_{0.5-8\,\text{keV}}^{\text{tot}}(\text{erg s}^{-1}) \approx (3.5 \pm 0.4) \times 10^{39}\,\text{SFR}\,(M_\odot\,\text{yr}^{-1})\quad (3)$$

where the uncertainty was computed from the scatter of the points around the best fit. The results of all fits are summarized in Table 3.

The scale factor in eq. (3) is larger than the scale factor obtained for the collective luminosity of HMXBs in resolved galaxies (eq.(22) Paper I) by a factor of ~ 1.34. Therefore, we can conclude, that the unresolved emission contributes, in average, $\sim 1/4$ of the total X-ray luminosity of star-forming galaxies generated per unit of SFR. This result is consistent with the preliminary estimate obtained in the Paper I based on the comparison of the $L_X - $ SFR relations of the HMXBs in the resolved galaxies and total emission from unresolved galaxies. It is also consistent with the scaling relation for the ISM emission obtained in the Paper II.

In the conclusion of this section we note that the result of the fitting of the $L_X - $ SFR relation depends on whether the fit was performed in the logarithmic or linear space. In the linear case, it also depends on whether the least square fit in the form $L_X = A \times$ SFR was performed or individual $L_X/$SFR ratios were averaged (note that in the log case it is same). Note also that large scatter of points, much bigger than statistical uncertainties, renders the χ^2 minimization less appropriate. Doing the least square fit to the linear quantities, we obtain the scale of $L_X/\text{SFR} \approx (2.7 \pm 0.2) \times 10^{39}$ (erg s^{-1})/$(M_\odot$ yr$^{-1})$. Averaging the $L_X/$SFR ratio in the linear space, we obtain yet another number: $L_X/\text{SFR} \approx (5.0 \pm 0.6) \times 10^{39}$ (erg s^{-1})/$(M_\odot$ yr$^{-1})$, i.e. nearly twice larger than in the eq.(3). The value obtained in the logarithmic fit is smaller, because it gives equal weights to the low and high points.[2] As this seems to be a more correct approach and in order to be consistent with the Paper I, we used the fit in the log space as default.

[2] Indeed, for two measurements yielding $y_1 = a$ and $y_2 = 10\,a$ the logarithmic (geometrical) average is $\langle y \rangle_{log} \approx 3.16\,a$ while the linear average is $\langle y \rangle_{lin} = 5.5\,a$, i.e. is nearly twice larger.

4.1 Comparison with previous results

Ranalli, Comastri, & Setti (2003) studied the $L_X - $ SFR relation using X-ray data from ASCA and BeppoSAX satellites. In the Paper I, we converted their X-ray luminosity and SFR to make them consistent with the analogous quantities used here and derived: $L_{0.5-8\,\text{keV}} \approx 1.6 \cdot 10^{39} \times$ SFR, i.e. more than ~ 2 times smaller than our eq.(3). The rather large discrepancy is likely caused by the confusion in the definition of SFR proxies (see detailed discussion in the Paper I). On the other hand, the $L_X - L_{IR}$ relation of Ranalli, Comastri, & Setti (2003), transformed to be compatible with our definitions is $L_{0.5-8\,\text{keV}} \approx 2.4 \cdot 10^{-4} \times L_{IR}$. The scale in this relation is $\approx 27\%$ larger that the scale in the corresponding relation for HMXBs from the Paper I (eq.(23)), consistent with $\sim 1/4$ contribution of hot ISM and other unresolved emission components to the total luminosity – see the discussion after the eq.(3) above. This proves that the underlying $L_X - L_{IR}$ relations are fully compatible and the discrepancy in the $L_X - $ SFR relation is due the difference in the use and definitions of SFR proxies.

Persic & Rephaeli (2007) investigated the relation between the total X-ray emission from normal and starburst (ULIRGs) galaxies in the 2–10 keV band and the SFR derived from infrared luminosity. Using their eq. (10) and converting the 2–10 keV luminosity to the 0.5–8 keV band (a factor of 1.28) we obtain: $L_{0.5-8\,\text{keV}} \approx 4.9 \cdot 10^{39} \times$ SFR. This relation is consistent, within a factor of ~ 1.4 with our eq. (3). On the other hand, in the Paper I we found a rather large disagreement between our $L_X - $ SFR relations for the HMXB luminosity.

Lehmer et al. (2010) recently studied the relation between 2–8 keV luminosity and SFR for a sample of nearby LIRGs using *Chandra* observations. They obtained the hard band luminosities by modeling the X-ray spectra in 0.5–8 keV band using Galactic absorption, a thermal component and a power-law component. This is consistent with the model we used to fit the X-ray spectra of our sample of LIRGs and ULIRGs and determine their X-ray luminosities. In order to compare our results with the $L_X - $ SFR relation obtained by Lehmer et al. (2010), we converted their 2–8 keV luminosity to the 0.5–8 keV band. We assumed same model as above, with average quantities from our ULIRGs spectral fits ($\Gamma \sim 1.7$, $kT \sim 0.6$ keV, $N_H \sim 2 \times 10^{21}$ cm^{-2}
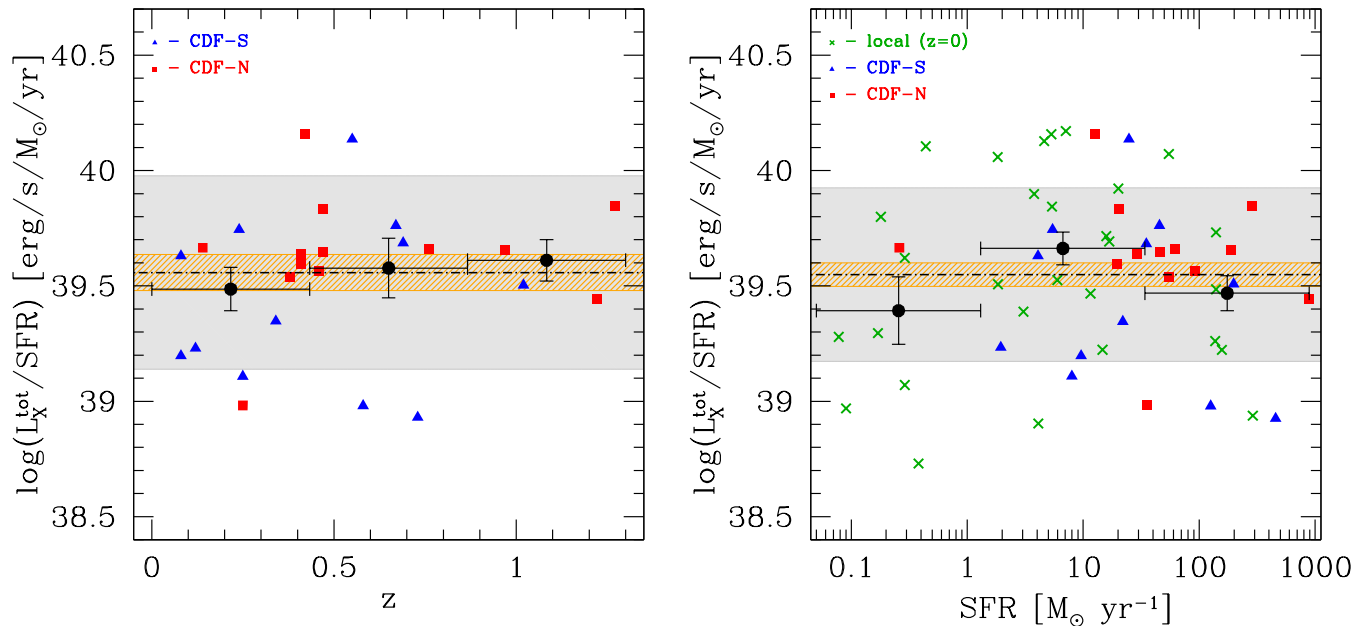
Figure 3. Dependence of the $L_X^{tot} - $ SFR relation on redshift (left panel) and star formation rate (right panel). The symbols without error bar indicate individual galaxies. The (black) filled circles with error bars show their average values within each redshift (left) or SFR (right) bin. The vertical error bars are uncertainties of the average values computed from the *rms* of points in the given bin. In the left panel, the horizontal dot-dashed line shows the average local L_X^{tot}/SFR ratio. Its uncertainty is shown by the narrower (orange) shaded area, while the wider (grey) shaded area shows the *rms* of the points. On the right hand panel, the horizontal line and the shaded areas show similar quantities computed using all galaxies.

and thermal-to-power-law normalization ratio of ~ 0.5). For the linear (first line in their Table 4) $L_X - $ SFR relation in Lehmer et al. (2010) we obtain a scale factor $L_X/\text{SFR} \approx 2.9 \times 10^{39}$ $(\text{erg s}^{-1})/(M_\odot \text{ yr}^{-1})$. This result is also in a reasonable agreement with our eq. (3).

5 CONSTRAINTS ON THE REDSHIFT AND SFR DEPENDENCE OF THE $L_X - $ SFR RELATION

The composition of the sample (29 galaxies at the redshift $z = 0$ and 25 galaxies at $z \approx 0.1 - 1.3$) allows us to constrain a possible redshift evolution of the X-ray emission produced per unit SFR. To this end, we grouped the CDF galaxies into three redshift bins of the equal width spanning from $z = 0$ to $z = 1.3$ and computed the average L_X^{tot}/SFR ratio and its uncertainty within each bin. Same quantities were computed for the local sample of galaxies, to characterize the $z = 0$ population. The result of this calculation is shown in Fig. 3. It is evident from the figure, that the average values for CDF galaxies are consistent, within uncertainties, between each other and with the average quantity for local galaxies. To confirm this, we applied the Spearman's rank test and we found no statistically significant correlations, neither for the individual values not for the average points, with the corresponding probabilities of $P \sim 27\%$ and $P \sim 20\%$ respectively.

Thus, the total X-ray emission produced per unit SFR by late-type galaxies does not show statistically significant trends with the redshift up to $z \sim 1.3$. The sensitivity of

this analysis is sufficient to eliminate the changes larger than $\sim 0.1 - 0.2$ dex (by factor of $\sim 1.3 - 1.6$), although as a caveat we should note that the high redshift bin contained only 4 galaxies. This conclusion is in agreement with results of the X-ray stacking analysis of late-type galaxies (Lehmer et al. 2008) and with calculations of the maximal contribution of star-forming galaxies to the unresolved CXB intensity (Dijkstra et al. 2012).

Recent population synthesis calculations by Fragos et al. (2012) predict that the ratio of the 0.5–8 keV luminosity to the SFR increases by a factor of $\sim 1.3 - 1.4$ between redshift $z = 0$ and $z \sim 1.3$. Such an evolution is within the uncertainties of our results.

Finally, in the right hand panel of the Fig.3 we constrain the possible dependence of the L_X/SFR ratio on the SFR. Using both local and CDF galaxies, we bin the data into 3 SFR bins and compute the average and its uncertainty (*rms*-based) for each redshift bin. The formal $\chi^2 = 4.8$ for the binned data, with 2 dof. The probability of having such (or bigger) value of the χ^2 is $\sim 9\%$, which is equivalent to $\sim 1.5\,\sigma$ detection. This may or may not indicate the existence of some SFR dependence in the $L_X - $ SFR ratio. If any, the amplitude of this dependence also does not exceed ~ 0.15 dex (a factor of ~ 1.4). Finally, we note that due to the observer's bias, the effect of statistics of the small numbers (Gilfanov, Grimm, & Sunyaev 2004) is not strong in our sample.

6   SUMMARY

Based on the sample of nearby resolved galaxies more distant ULIRGs at intermediate distances and star-forming galaxies from the *Chandra* Deep Fields, we construct a sample of 54 star-forming galaxies spanning the range of redshifts from $z = 0$ up to $z = 1.3$ and the range of star formation rates SFR $\sim 0.1 - 10^3$ M$_\odot$/yr (Fig.1). Using this sample, we calibrate the $L_X - $ SFR relation for the 0.5–8 keV band luminosity (Fig.2). We find that $L_X - $ SFR dependences for the local and CDF samples are consistent with linear relations with the typical accuracy of ~ 0.1 in the slope. The linear $L_X - $ SFR relation obtained for the entire sample is given by the eq.(3). We did not find any statistically significant trends in the scaling relation with the redshift and star formation rate with the upper limit on the possible variations in the L_X/SFR ratio of $\sim 0.1 - 0.2$ dex (a factor of $\sim 1.3 - 2.6$) (Fig.3). This property makes the X-ray emission a powerful tool to measure star formation rate in a broad range of redshifts and star formation regimes, which can be applied *en masse* to faint distant galaxies.

REFERENCES

Bell E. F., 2003, ApJ, 586, 794
Bundy K., Ellis R. S., Conselice C. J., 2005, ApJ, 625, 621
Condon J. J., 1992, ARA&A, 30, 575
Cowie L. L., Barger A. J., Hasinger G., 2012, ApJ, 748, 50
Dijkstra M., Gilfanov M., Loeb A., Sunyaev R., 2012, MN-RAS, 421, 213
Drozdovsky I. O., Karachentsev I. D., 2000, A&AS, 142, 425
Drozdovsky I. O., Schulte-Ladbeck R. E., Hopp U., Greggio L., Crone M. M., 2002, AJ, 124, 811
Fragos T., et al., 2012, arXiv, arXiv:1206.2395, submitted to ApJ
Giavalisco M., et al., 2004, ApJ, 600, L93
Gilfanov M., Grimm H.-J., Sunyaev R., 2004, MNRAS, 351, 1365
Grimes J. P., Heckman T., Strickland D., Ptak A., 2005, ApJ, 628, 187
Grimm H.-J., Gilfanov M., Sunyaev R., 2003, MNRAS, 339, 793
Grisé F., Pakull M. W., Soria R., Motch C., Smith I. A., Ryder S. D., Böttcher M., 2008, A&A, 486, 151
Ismail H. A., Alawy A. E., Takey A. S., Issa I. A., Selim H. H., 2005, JKAS, 38, 7
Kellermann K. I., Fomalont E. B., Mainieri V., Padovani P., Rosati P., Shaver P., Tozzi P., Miller N., 2008, ApJS, 179, 71
Kroupa P., 2001, MNRAS, 322, 231
Li J.-T., Wang Q. D., 2012, arXiv, arXiv:1201.0551
Lehmer B. D., et al., 2008, ApJ, 681, 1163
Lehmer B. D., Alexander D. M., Bauer F. E., Brandt W. N., Goulding A. D., Jenkins L. P., Ptak A., Roberts T. P., 2010, ApJ, 724, 559
Lehmer B. D., et al., 2012, ApJ, 752, 46
Makarova L. N., Karachentsev I. D., 2003, Ap, 46, 144
Mineo S., Gilfanov M., Sunyaev R., 2011, AN, 332, 349
Mineo S., Gilfanov M., Sunyaev R., 2012, MNRAS, 419, 2095 (Paper I)
Mineo S., Gilfanov M., Sunyaev R., 2012, arXiv, arXiv:1205.3715 (Paper II), submitted to MNRAS
Persic M., Rephaeli Y., 2007, A&A, 463, 481
Ranalli P., Comastri A., Setti G., 2003, A&A, 399, 39
Richards E. A., 2000, ApJ, 533, 611
Saha A., Thim F., Tammann G. A., Reindl B., Sandage A., 2006, ApJS, 165, 108
Sanders D. B., Mazzarella J. M., Kim D.-C., Surace J. A., Soifer B. T., 2003, AJ, 126, 1607
Sakai S., Madore B. F., 1999, ApJ, 526, 599
Saviane I., Hibbard J. E., Rich R. M., 2004, AJ, 127, 660
Schmitt H. R., Calzetti D., Armus L., Giavalisco M., Heckman T. M., Kennicutt R. C., Jr., Leitherer C., Meurer G. R., 2006, ApJ, 643, 173
Taylor E. N., et al., 2009, ApJS, 183, 295
Tully R. B., 1988, Sci, 242, 310
Tully R. B., Rizzi L., Shaya E. J., Courtois H. M., Makarov D. I., Jacobs B. A., 2009, AJ, 138, 323
Willick J. A., Courteau S., Faber S. M., Burstein D., Dekel A., Strauss M. A., 1997, ApJS, 109, 333
Zibetti S., Charlot S., Rix H.-W., 2009, MNRAS, 400, 1181
Xue Y. Q., et al., 2011, ApJS, 195, 10

This paper has been typeset from a TEX/ LATEX file prepared by the author.